Theoretical and experimental study of the magnetic structure of TlCo$_2$Se$_2$

Raquel Lizárraga,[1] Sabina Ronneteg,[2] Rolf Berger,[2] Anders Bergman,[1] Peter Mohn,[3] Olle Eriksson,[1] and Lars Nordström[1]

[1]*Department of Physics, Ångström Laboratory, Uppsala University, Box 530, S-751 21, Uppsala, Sweden*
[2]*Department of Materials Chemistry, Ångström Laboratory, Uppsala University, Box 538, S-751 21, Uppsala, Sweden*
[3]*Department of Physics, University of Technology CMS A-1040, Vienna, Austria*

The magnetic properties of TlCo$_2$Se$_2$ are investigated by means of single-crystal neutron diffraction experiments and first principles calculations. The previous suggestion of a noncollinear incommensurate magnetic structure based on powder neutron diffraction data is confirmed by single-crystal diffraction. Our theoretical calculations find that TlCo$_2$Se$_2$ adopts an antiferromagnetic ordering. The magnetism is dominated by the contribution from the Co atoms, where the magnetic moments are arranged ferromagnetically within the ab plane. The magnetic moments from experiments are reproduced very well by our theoretical calculations. The origin of the magnetic ordering is analyzed by a detailed inspection of the energy band structure and the Fermi surface. The small calculated energy difference (≈ 0.1 mRy) between the two magnetic arrangements, the experimental noncollinear and the antiferromagnetic, is viewed as the most likely origin of this discrepancy. The influence of nonstoichiometric samples on the magnetic state is also argued to be a possible source for the observed small discrepancy between experiment and theory.

PACS number(s): 75.50.$-$y, 71.20.Be, 71.15.Mb

I. INTRODUCTION

Low dimensionality can lead to extremely subtle and complex magnetic behavior in solids. Particularly interesting is the case where the type of ordering is very sensitive to both atomic distances and composition. Very often these systems are studied in compounds with the general formula AT$_2$X$_2$. The crystal structure adopted by these systems is the layered tetragonal ThCr$_2$Si$_2$-type (space group I4/mmm), where the T atoms sit on a square lattice in two dimensions (Fig. 1). There exists some 700 compounds of this structure type (for a review see Ref. 1) and their structural properties,[2,3] electronic structure and magnetism[4–8] have in several cases been investigated.

Systems formed by nonmagnetic and large A and X atoms would enhance the two-dimensional character of these materials. However, only a few studies have been reported in the literature for such "quasi-two-dimensional" systems. By choosing thallium (or an alkali metal) for the A atom and sulfur, selenium or tellurium for the X atom such conditions are fulfilled.[9,10] The distance between consecutive layers of T atoms is large, of the order of 7 Å. The interatomic T–T distances within the layers (square coordination) are of the same order as in the transition metals, just below 2.8 Å. TlCo$_2$Se$_2$ is an example of such systems and recently this compound has been extensively investigated.[11] Newmark *et al.*[12] proposed an antiferromagnetic ordering that was confirmed by Berger *et al.*,[11] however, the simple model of antiparallel coupling between spins in adjacent layers[12] based on magnetization measurements was refuted. Powder neutron diffraction data[11] indicated an incommensurate helix running along the c axis with a turn angle of $\sim 121°$. The magnetic moments of the cobalt atoms are ferromagnetically ordered within each layer and perpendicular to the c axis. The helical wave vector was found to be $(0,0,q)$ with $q \sim 0.3$ and the moment on Co atoms was 0.46 μ_B.

The magnetic and crystal structures of TlCo$_2$Se$_2$ are depicted in Fig. 1 (the magnetic cell displayed in the figure contains only the Co atoms that carry the magnetism in this compound). This kind of noncollinear magnetic structure has not been reported for Co-based systems before. To our knowledge TlCo$_2$Se$_2$ is the only Co-based compound with a noncollinear magnetic structure, and a natural question to ask is of course why this is the case. It should be noted here that noncollinear magnetic states are mostly found for Mn and in some cases Fe-based compounds.[13] Indeed, there have been several noncollinear magnetic structures reported for Mn-based compounds with the ThCr$_2$Si$_2$-type structure.[14–16]
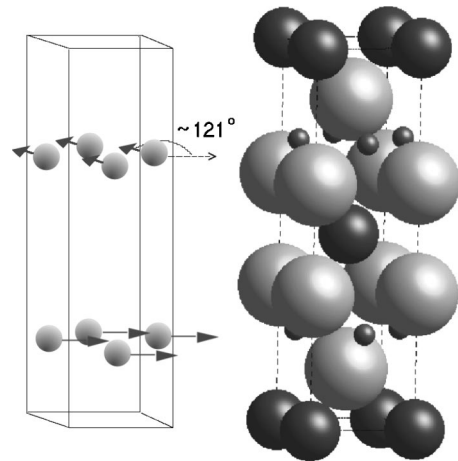

FIG. 1. The experimental magnetic structure of the TlCo$_2$Se$_2$ compound and the body centered tetragonal (bct) crystal structure are depicted in the figure. The magnetic moments of the cobalt atoms (small spheres) are arranged ferromagnetically within each layer and perpendicular to the c axis. An incommensurate helix runs along the c axis with a turn angle of $\sim 121°$, as it is indicated by the arrows on the cobalt atoms. The Tl atoms are shown as large dark spheres whereas the Se atoms are shown as large light spheres.

In the present study, we have investigated $TlCo_2Se_2$, combining single crystal neutron diffraction with theoretical first principles calculations. Since the experimental model proposed by Berger *et al.*[11] could not distinguish between the helical magnetic structure and sine-modulated moments, a single-crystal investigation was suggested. Moreover, single-crystal data give, in general, more spatial information as compared to powder diffraction.

Our theoretical analysis of the magnetic structure of $TlCo_2Se_2$ was performed using a first principles method based on the full potential augmented plane wave method with local orbitals (APW+lo).[17,18] Our noncollinear scheme[18] treats the magnetization density as a vector field that is free to vary both in magnitude and direction throughout space. Moreover, the spin spiral symmetry is adopted that allows us to use the chemical unit cell regardless of the size of the magnetic cell. Therefore, it is ideally suited for the present investigation. It should be noted here that the presently used theoretical method has been tested thoroughly for rare-earth systems[6,19] as well as for fcc Fe.[20]

II. EXPERIMENTS

A. Synthesis

The $TlCo_2Se_2$ crystal was synthesized by mixing stoichiometric amounts of TlSe, Se shots, and Co powder. The materials were brought to melting in an evacuated silica tube and then slowly cooled to room temperature.[21] The solidified ingot showed strong preferred orientation and split easily through cleavage by a scalpel. The crystal had a crescent shape, almost a flat half circle, approximately of a diameter of 8.8 mm and a thickness of 0.4 mm. The flat surfaces were of the (0 0 1) orientation.

B. Single crystal diffraction analysis

The quality of the $TlCo_2Se_2$ crystal was ascertained by x-ray diffraction (Philips X'pert system, parallel beam optics, mirror/mirror, $CuK\alpha$), by verifying the fourfold symmetry of the (1 0 11) reflection using a Phi scan, and using a rocking-curve geometry on the (0 0 8) plane for the domain quality.

The neutron diffraction measurement was performed on the Single Crystal Diffractometer (SXD) in Studsvik, Sweden. Five magnetic peaks and 60 to 90 nuclear reflections were collected in each set at 45, 60, and 80 K, all below T_N. Lower temperatures could not be reached due to a refrigeration failure.

The data reduction was first carried out using the ARACOR program for extracting the intensities from the background.[22] The intensities were corrected for Lorentz and absorption effects, using the program ABSSTOE.[22] The reduced data set was made into an intensity file for the program Fullprof.[23]

This strategy makes it possible to refine the magnetic moment of the cobalt atom. The intensity file contains the propagation vector, *hkl* indices, net intensity with standard deviation, and the scale factor. The temperature factors and the atom positions were refined using only the nuclear peaks and these values were then fixed during the magnetic refine-
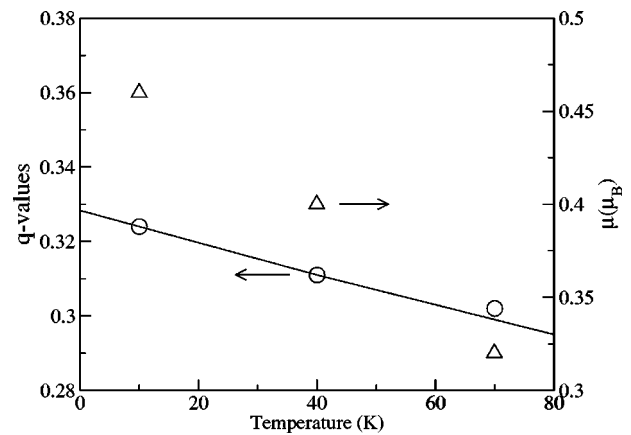

FIG. 2. Results of the q value in $(0,0,1\pm q)$ ($\bigcirc$) and the magnetic moment of the cobalt atoms ($\triangle$) from the powder neutron refinement done by Berger *et al.* (Ref. 11). Axes are indicated by arrows.

ment. In this refinement method, it is not possible to refine the propagation vector and the cell parameters. Therefore, the q value for the propagation vector and the cell parameters were fixed using values from the powder Rietveld refinements made by Berger *et al.*[11] Since the single-crystal neutron diffraction measurements were not performed at the same temperatures as for the earlier powder diffraction data collection, linear inter- and extrapolation was applied (Fig. 2).

III. THEORETICAL METHOD

Our theoretical calculations have been performed using a noncollinear method implemented in the alternative linearization of the full-potential augmented plane wave method (FP−APW+lo).[17] The local density approximation (LSDA) in a noncollinear scheme, as parametrized by von Barth and Hedin,[24] was used. The magnetization density is treated as a vector field, being free to change both in magnitude as well as in direction throughout space.[18] The spin spiral (SS) symmetry[25,26] was incorporated in order to handle a planar
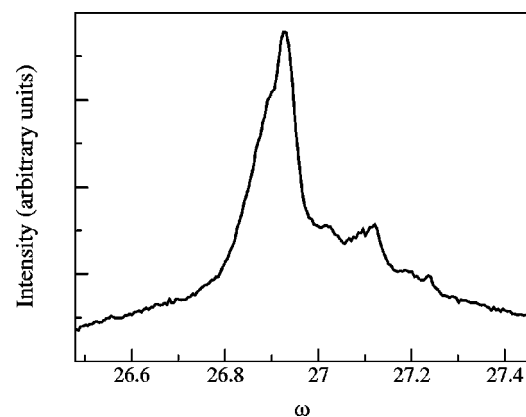

FIG. 3. X-ray diffraction rocking curve on the (0 0 8) reflection of the crystal used for the neutron diffraction.

TABLE I. Refinement results of the single-crystal neutron diffraction experiments. The values are the relative intensities (arbitrary units). Both observed (obs.) and calculated (calc.) values are given.

hkl	45 K		60 K		80 K	
	obs.	calc.	obs.	calc.	obs.	calc.
(001^+)	47(5)	47(7)	38(3)	42(7)	12(2)	17(4)
(003^-)	41(5)	41(6)	36(3)	37(6)	15(2)	15(4)
(003^+)	40(6)	38(6)	26(3)	33(6)	11(3)	14(4)
(005^-)	27(6)	29(5)	29(3)	25(5)	14(4)	10(3)
(111^-)	14(7)	14(4)	10(4)	12(3)	3(3)	5(2)
(111^+)	13(7)	14(1)	10(3)	12(3)	2(3)	5(2)
$(013)^a$	$1.123(7) \times 10^4$	$1.11(4) \times 10^4$	$1.111(7) \times 10^4$	$1.12(1) \times 10^4$	$1.100(7) \times 10^4$	$1.11(1) \times 10^4$

^{a}The strongest nuclear peak on the same intensity scale for a comparison.

helical spin structure with wave vector $\mathbf{Q}=(0,0,Q)$, where the parallel spins within a plane are rotating around the spiral axis with an angle $\phi=Qc/2$ between each plane. When including the SS symmetry the magnetization density is not translational invariant. A generalized boundary condition must be used

$$\mathbf{m}(\mathbf{r} + \mathbf{R}) = \mathcal{D}(\mathbf{Q} \cdot \mathbf{R})\mathbf{m}(\mathbf{r}), \qquad (1)$$

where $\mathbf{R}$ is a Bravais lattice vector, and $\mathcal{D}(\mathbf{Q} \cdot \mathbf{R})$ is a matrix that accomplishes a rotation of the in-plane component of $\mathbf{m}$ by the angle $\mathbf{Q} \cdot \mathbf{R}$ around the tetragonal axis. The generalized Bloch spinor states can then be written as[25]

$$\psi_{\mathbf{k}}(\mathbf{r}) = \begin{pmatrix} e^{i(\mathbf{k}-\mathbf{Q}/2)\cdot\mathbf{r}} \alpha_{\mathbf{k}}(\mathbf{r}) \\ e^{i(\mathbf{k}+\mathbf{Q}/2)\cdot\mathbf{r}} \beta_{\mathbf{k}}(\mathbf{r}) \end{pmatrix}, \qquad (2)$$

where $\mathbf{k}$ is a wave vector in the Brillouin zone (BZ) and α and β are the periodic functions for the spin-up and spin-down components, respectively. The secular matrix constructed from theses states is, in general, not block diagonal, which means that the two spin components can hybridize. Self-consistency is achieved by constructing new charge and magnetization densities from the occupied Bloch spinors. This SS scheme permits us to take into account noncommensurate orderings in a natural fashion,[19] avoiding using supercells.

We used the lattice constants, a and c, of the body-centered tetragonal (bct) structure of $TlCo_2Se_2$ determined experimentally by Berger *et al.* at the lowest temperature.[11] BZ integrations are performed using a mesh of 320 $\mathbf{k}$ points in the irreducible first Brillouin Zone.

IV. EXPERIMENTAL RESULTS

A ϕ scan of the flat crystal showed four peaks of the {1 0 11} type, confirming the fourfold symmetry. However, the rocking curve shown in Fig. 3 indicates a mosaic structure manifested by a peak split of $\sim 0.2°$, probably related to dislocations in the crystal. The quality of the $TlCo_2Se_2$ crystal was sufficiently good, considering the large size.

The mosaic domains in the crystal result in a broadening of all diffraction peaks. The integrated intensities are all affected, influencing the refinement of the temperature factors.

Due to this, the values calculated for these parameters were anomalously high.

All the magnetic peaks in the neutron diffraction pattern have very small intensities due to the low moment. It was thus very unfortunate that the strongest reflection $(0\,0\,1^-)$ could not be accessed for measurement due to the instrumental geometry of the SXD. The collected magnetic peaks are listed in Table I.

In the single-crystal Fullprof refinement, all magnetic and nuclear peaks were used. The results of the magnetic moment and the R values are listed in Table II. Due to the very low intensities of the remaining magnetic peaks, it was not possible to refine the magnetic moment more accurately than in the powder diffraction experiments. Nevertheless, the value of the magnetic moments on the cobalt atom are consistent between the two diffraction approaches. It was also not possible to distinguish between the two different magnetic models, the helical structure and the sine-modulated moments, due to the very low intensity of the (111) satellites. The helical structure is more likely, simply because it is more prevalent among the transition metals. The values in Table II are to be compared with the data in Fig. 2. In this figure, the values of the magnetic moments from the powder neutron refinement[11] are plotted as a function of temperature. We may similarly use the intensities of the magnetic reflections collected in Table I for studying the temperature dependence

TABLE II. Refined parameters, lattice constants, q value, and magnetic moments, corresponding to the data in Table I.

	45 K	60 K	80 K
$a(\text{Å})$	3.8315	3.8315	3.8315
$c(\text{Å})$	13.440	13.446	13.454
q in $(001 \pm q)$	0.309	0.303	0.295
Q^a	0.691	0.697	0.705
μ of Co (μ_B)	0.7(2)	0.6(2)	0.4(2)
$R_{\text{crys}}(\%)$	4.94	6.86	5.92
$R_{\text{magn}}(\%)$	4.93	6.87	5.93

^{a}The Q values, where $\mathbf{Q}=(0,0,Q)2\pi/c$ is the wave vector of the spin spiral, correspond to the notation used in the theoretical part of this paper and are given here as well in order to make the comparison between experiment and theory easier ($Q=1-q$).
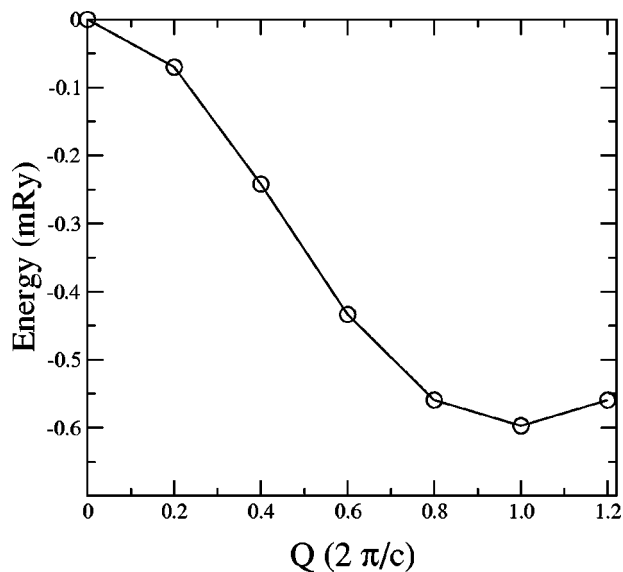
FIG. 4. The total energy as a function of the spin spiral wave vector $\mathbf{Q}=(0,0,Q)2\pi/c$, relative to the energy of the ferromagnetic structure ($Q=0$).

FIG. 5. The calculated charge (left) and spin density (right) of $TlCo_2Se_2$ in the (010) plane, for a ferromagnetic coupling of the Co atoms.

of the moments. We were not able to refine the q values from the single-crystal data, but by using the values expected, we obtained reasonable fits as seen from the R values in Table II.

V. THEORETICAL RESULTS

Several magnetic orders have been investigated which correspond to ordering vectors along the (0,0,1) direction of the Brillouin zone of the bct structure. The calculated total energies of these magnetic structures as a function of the helical ordering, $\mathbf{Q}=(0,0,Q)2\pi/c$ that characterizes them, are displayed in Fig. 4. The ordering vectors $Q=0$ and $Q=1$ correspond to the ferromagnetic and the antiferromagnetic order, respectively. In Fig. 4, the total energy curve presents a minimum at the wave vector, $Q=1$, which means that the antiferromagnetic structure is energetically favored (note that the energies are given with respect of the energy of the ferromagnetic state). It is interesting to note that the calculated energy difference between the helimagnetic state found experimentally (at $Q\approx0.7$) and the antiferromagnetic state determined theoretically as the ground state is very small, ≈0.1(mRy).

The magnetic moments were also calculated. The main contribution to the magnetic moments comes from Co atoms and is $0.51\ \mu_B$/atom. This agrees reasonably well with both our current experimental data, $0.7(2)\mu_B$/atom and the previous powder neutron diffraction result $0.46(2)\mu_B$/atom.[11] Thallium and selenium atoms have no significant contribution to the total magnetic moment, $0.01\ \mu_B$ and $0.0\ \mu_B$, respectively. This can be seen in Figs. 5 and 6. On the right side of Fig. 5 we present the spin density for the (010) plane for a ferromagnetic coupling. The magnetization density is high at the two Co atoms in this plane of the crystal structure, being almost zero at the Tl and Se sites. On the left side of Fig. 5 we also show the charge density.
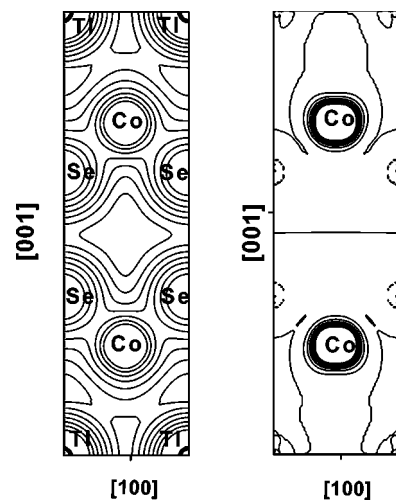
One may notice that the density is spherical around the Tl, Co, and Se atoms, but that it has large regions where it is nonspherical, which reflects the rather open nature of this crystal structure. In connection to this observation it is relevant to compare the current results with those of our previous calculation based on the linear muffin-tin orbitals method within the atomic sphere approximation (LMTO-ASA), in an implementation that allows for the handling of noncollinear systems.[27] These calculations[28] showed that a SS with $\mathbf{Q}\approx(0,0,0.57)2\pi/c$ had the lowest energy in rather good agreement with experiment. However, due to the rather open nature of the crystal lattice (revealed by the charge density, shown in Fig. 5), it stands clear that the atomic sphere approximation becomes less accurate. In fact, the sphere overlap was approaching the limit where the ASA
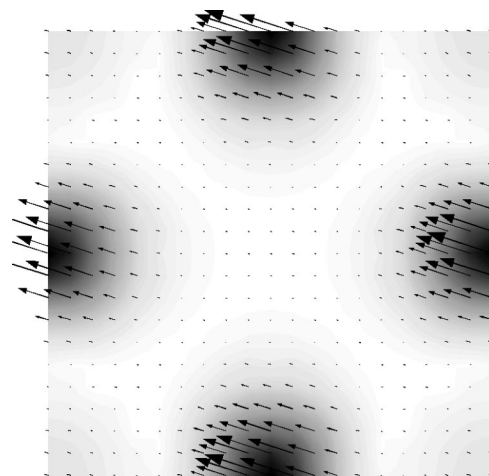

FIG. 6. The calculated magnetization density, shown in a gray scale. A darker shade stands for higher density. The plane displayed in the figure corresponds to an ab plane of the conventional cell at $z=c/4$, the plane that contains the Co atoms. Noncollinear directions are represented by arrows.
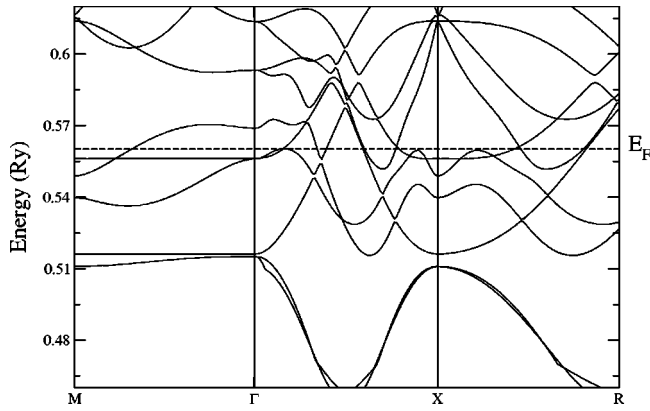
FIG. 7. The calculated band structure of a spin spiral with $\mathbf{Q}$ $=(0,0,0.7)2\pi/c$ along three directions of the Brillouin zone.
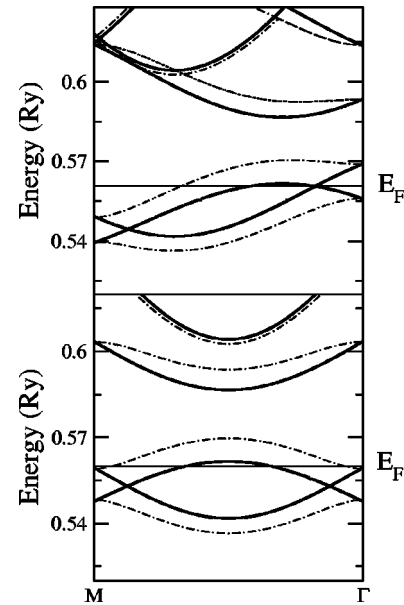

FIG. 8. Band structures of $TlCo_2Se_2$. The upper panel shows the band structures of the ferromagnetic state (solid lines) and a SS with $\mathbf{Q}=(0,0,0.7)2\pi/c$ (dash-dotted). In the lower panel, the solid line corresponds to the band structure of the ferromagnetic state and the dash-dotted indicates the band structure of the antiferromagnetic state. It should be noted that we show only the bands that changes the most when $\mathbf{Q}$ is modified.

approximation becomes less accurate,[29] especially considering the very small energies that are involved for resolving the correct magnetic structure.

In Fig. 6 we show the calculated magnetization density of a SS whose wave vector is $\mathbf{Q}=(0,0,0.7)2\pi/c$. The depicted plane corresponds to an ab plane of the conventional cell (bct) at $z=c/4$, which actually contains the Co atoms. In this figure, a darker shade indicates higher magnetization density, precisely located at the cobalt atom sites. The magnetization density, projected in the xy plane is depicted by arrows, where the length of the arrows corresponds to the magnitude of the vector. The magnitude of the magnetization density is appreciable only where the cobalt atoms are placed and they order ferromagnetically within the plane that contains them.

VI. ELECTRONIC STRUCTURE

Figure 4 clearly indicates that although the antiferromagnetic order minimizes the total energy, any of the SS configurations studied has lower energy than the ferromagnetic state. We present here an analysis of the electronic structure in order to investigate the possible stabilization of a SS state. Two bands in the ferromagnetic configuration of opposite spin character that cross each other can hybridize in the SS state. The hybridization of these two bands gives rise to a splitting of them. Hence, one band is pushed down lowering the total energy and the other is pushed up. If these bands are crossing at, or close to the Fermi energy, the band that is shifted up becomes unpopulated, making no contribution to the total energy. This is a mechanism of lowering the energy[13,30] that favors the formation of spin spirals. The mixing of the spin up and down states that always occurs in the SS symmetry reduces the magnetic moments compared with the ferromagnetic state, increasing the exchange energy. This increase in exchange energy can slightly compensate the lowering of the band energy. However, if the Fermi surface nesting is sufficiently strong, i.e., there are almost parallel sheets in the Fermi surface of the ferromagnetic system that are connected by a wave vector $\mathbf{Q}$, the mechanism sketched above is capable of stabilizing a SS structure with a wave vector $\mathbf{Q}$.

In order to explore this scenario, we show in Fig. 7 the band structure of $TlCo_2Se_2$ in the SS state (solid line) with $\mathbf{Q}=(0,0,0.7)2\pi/c$ along three directions of the Brillouin zone. However, in order to present a clear picture and facilitate the understanding of our analysis we have chosen to plot only the bands along the $\overrightarrow{M\Gamma}$ direction (parallel to $\mathbf{Q}$) in Fig. 8. The upper panel of Fig. 8 displays the ferromagnetic (dark solid line) and the SS bands with $\mathbf{Q}=(0,0,0.7)2\pi/c$ (dash-dotted line), while in the lower panel of the figure the ferromagnetic bands are compared with the bands of the antiferromagnetic configuration (dash-dotted line). The Fermi level is indicated in both panels by a thin solid line. It is worth noticing that the ferromagnetic bands (dark solid lines) in the upper and the lower part of the figure do not look the same. This is due to shape of the spin spiral wave function [see Eq. (2)] in which the spin-up and spin-down components are shifted $\pm Q/2$, respectively. Therefore in order to represent a ferromagnetic state with this wave function, either the wave vector $Q=0$ is used or the polar angles θ and ϕ that describe the direction of the magnetization density are set to zero with an arbitrary Q. Thus, in the upper panel, the ferromagnetic state was represented by $Q=0.7$ and the polar angles $\theta=\phi$ $=0$. This was done in order to compare with the band structure of the SS of wave vector $Q=0.7$. In a similar way, the ferromagnetic state in the lower panel of the Fig. 8 was described by $Q=1$ and $\theta=\phi=0$ to compare with the band structure of the antiferromagnetic $(Q=1)$ configuration. Hence, the band structure of the ferromagnetic state in both panels have a different Q shift, which makes them appear different. It is important to stress that the total energy is the same for
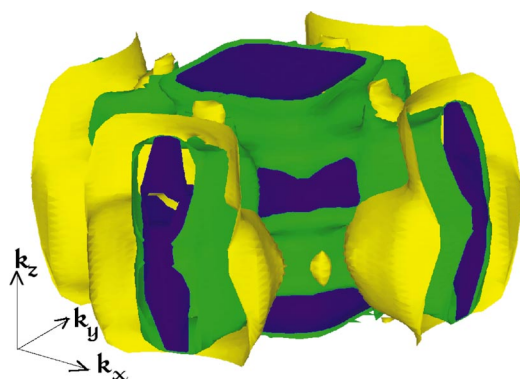
FIG. 9. (Color) Fermi surfaces of the ferromagnetic and the noncollinear state of the $TlCo_2Se_2$ compound. Spin-up and spin-down Fermi surfaces of the ferromagnetic state are depicted in blue and yellow, whereas the noncollinear Fermi surface is displayed in green.

these two cases, corresponding to the ferromagnetic state. The difference between the two ferromagnetic band structures is simply an effect of the form of the wave functions of SS [Eq. (2)] and may be seen as different representations of the same magnetic state.

In the upper panel of Fig. 8, there are two bands of the ferromagnetic system (dark solid line) close to the Fermi energy that cross each other twice. In contrast, these two bands in the SS configuration (dash-dotted) have hybridized and split. The higher band has moved up and the other band has moved down, below the Fermi energy lowering the total energy. In the lower panel of Fig. 8, the antiferromagnetic spin-up and spin-down bands do not cross each other near the Fermi energy. They rather look like the SS bands. It is worth noticing that, according to Fig. 8, the lowering energy mechanism described above would be more effective for the antiferromagnetic bands than for the SS system, since the band that has been pushed up is completely empty in the former case. This would explain the antiferromagnetic ground state found by our calculations. Moreover, one could speculate that a small error in determining the Fermi energy, due to the small energies involved, would lead to a different ground state. It is also possible that a slight deviation from stoichiometry in the experimental samples might shift the Fermi level such that the antiferromagnetic state becomes unstable toward a SS geometry, giving a possible mechanism for the small difference between experiment and theory.

To analyze further the mechanism for stabilizing noncollinear magnetic states, it is motivated to explore the Fermi surface of $TlCo_2Se_2$, of the ferromagnetic and noncollinear state. The presence of strong nesting in the Fermi surface is a good indicator that the mechanism mentioned above is capable to stabilize a SS structure. In Fig. 9 we display the Fermi surfaces of the ferromagnetic and the noncollinear state corresponding to the energy band plot in Fig. 8. We have chosen to display the energy bands that cross the Fermi energy in the $\overrightarrow{\Gamma M}$ direction, since for these bands, Fig. 8 suggests that a large difference of the Fermi surface should be observed between the ferromagnetic and noncollinear state. The spin-up and spin-down sheets of the ferromagnetic

configuration are shown in blue and yellow color, respectively. These two bands, that are not allowed to hybridize in the ferromagnetic configuration, can merge into one Fermi surface for the noncollinear state, which results in the green Fermi surface. Not all of the features of the ferromagnetic Fermi surface are visible due to the fact that we have overlaid the noncollinear Fermi surface in Fig. 9. However, a close inspection of the different sheets in Fig. 9 shows that, in agreement with the energy band plot in Fig. 8, the noncollinear Fermi surface corresponds to the opening up of band gaps. The differences in the noncollinear Fermi surface are obvious over the whole Brillouin zone. As a result there is a rather large change in the topology of the Fermi surface and many k points are indeed taking part in the energy lowering mechanism.

VII. CONCLUSION

The interpretation of the previous powder neutron diffraction[11] was somewhat ambiguous due to the low intensities of the magnetic peaks, allowing for other possible explanations. The presently reported single-crystal study confirms the suggested noncollinear incommensurate magnetic structure of $TlCo_2Se_2$. However, our theoretical calculations find that the antiferromagnetic configuration is marginally lower in energy compared to the experimentally suggested magnetic structure. We explain this disagreement as the result of the small energies involved. The calculated ground stated differs from the experimental helimagnetic structure with ≈ 0.1 mRy. This fact demonstrates the complexity of the $TlCo_2Se_2$ compound and the sensitive dependence of the calculations on the approximation. Despite these facts, the calculated magnetic moment of the cobalt atoms was found to be 0.5 μ_B per atom and we found no significant contribution from the selenium and thallium atoms to the magnetic moment, which is in an almost perfect agreement with experiments. The single-crystal refinement could not, unfortunately, give an improved quality of the magnetic moments compared to the powder refinement, due to the inferior instrumental geometry of the diffractometer.

The stability of the noncollinear and the antiferromagnetic states over the ferromagnetic ordering was analyzed from the electronic structure. Both energy band plots and the calculated Fermi surface show a large topological change between the electronic structure of the ferromagnetic phase and the noncollinear phase. In particular, we find that some bands along the z direction of the reciprocal space cross the Fermi energy for the ferromagnetic configuration. Due to the formation of a SS geometry these bands are allowed to hybridize, which opens up an energy gap around the Fermi level. This has previously been analyzed to stabilize a noncollinear state, and the present result is consistent with the conclusions drawn in Ref. 30, namely that there are two criteria that need to be fulfilled in order to observe noncollinear magnetism in metals, i.e., the Fermi level needs to cut through both spin-up and spin-down bands and there should be strong nesting between the spin-up and spin-down Fermi surfaces.[31] This explains why $TlCo_2Se_2$ so far is the only Co-based compound with noncollinear magnetic ordering; for this compound the

magnetic moment is reduced (compared to hcp Co) due to hybridization with ligand states in such a way that the two criteria outlined above become operative. This analysis opens up the possibility to search for other magnetic systems with noncollinear magnetic ordering. Based on this analysis, one may speculate that a slight deviation of stoichiometry in the samples positions the Fermi level at a somewhat lower energy, such that the mechanism discussed around Fig. 8 becomes maximally operative for the SS with Q=0.7.

[1] G. Just and P. Pauffler, J. Alloys Compd. **232**, 1 (1996).

[2] A. Mewis, Z. Naturforsch. B **35B**, 141 (1980).

[3] P. Pilchowski and A. Mewis, Z. Anorg. Allg. Chem. **581**, 173 (1990).

[4] R. Hoffman and C. Zheng, J. Phys. Chem. **89**, 4175 (1985).

[5] C. Zheng and R. Hoffman, J. Solid State Chem. **72**, 58 (1988).

[6] P. Andersson, L. Nordström, P. Mohn, and O. Eriksson, Phys. Rev. B **65**, 174109 (2002).

[7] A. Continenza and P. Monachesi, J. Appl. Phys. **75**, 7027 (1994).

[8] L. M. Sandratskii and J. Kübler, Phys. Rev. B **50**, 9258 (1994).

[9] K. Klepp and H. Boller, Monatsch. Chem. **109**, 1049 (1978).

[10] G. Huan, M. Greenblatt, and M. Croft, Eur. J. Solid State Inorg. Chem. **26**, 193 (1989).

[11] R. Berger, M. Fritzsche, A. Broddefalk, P. Nordblad, and B. Malaman, J. Alloys Compd. **343**, 186 (2002).

[12] A. R. Newmark, G. Huan, M. Greenblatt, and M. Croft, Solid State Commun. **71**, 1025 (1989).

[13] J. Kübler, *Theory of Itinerant Magnetism* (Oxford Science Publications, Clarendon, New York, 2000).

[14] G. Venturini *et al.*, J. Magn. Magn. Mater. **150**, 197 (1995).

[15] G. Venturini *et al.*, J. Alloys Compd. **241**, 135 (1996).

[16] R. Welter *et al.*, J. Magn. Magn. Mater. **187**, 278 (1998).

[17] E. Sjöstedt, L. Nordström, and D. Singh, Solid State Commun. **114-1**, 15 (2000).

[18] L. Nordström and D. J. Singh, Phys. Rev. Lett. **76**, 4420 (1996).

[19] L. Nordström and A. Mavromaras, Europhys. Lett. **49**, 775 (2000).

[20] E. Sjöstedt and L. Nordström, Phys. Rev. B **66**, 014447 (2002).

[21] L. Norén, Research School of Chemistry, Australian National University, Canberra (private communication).

[22] J.O. Lundgren, Report UUIC-B14-405 , University of Uppsala, Sweden, Crystallographic Computing Programs, 1983.

[23] FullProf program by J. Rodriguez-Carvajal, L.L.B.C.-C., Saclay, France.

[24] U. von Barth and L. Hedin, J. Phys. C **5**, 1629 (1972).

[25] C. Herring, in *Magnetism IV*, edited by G. Rado and H. Suhl (Academic Press, New York, 1966), Chaps. 5, 13.

[26] L. M. Sandratskii, Adv. Phys. **47**, 91 (1998).

[27] The implementation of this code was the same as used in L. Bergqvist, P. A. Korzhavyi, B. Sanyal, S. Mirbt, I. A. Abrikosov, L. Nordström, E. A. Smirnova, P. Mohn, P. Svedlindh, and O. Eriksson, "Magnetic and electronic structure of $(Ga_{1-x}Mn_x)As$," Phys. Rev. B **67**, 205201 (2003).

[28] R. Lizárraga, S. Ronneteg, R. Berger, P. Mohn, L. Nordström, and O. Eriksson, Proceedings of the International Conference on Magnetism (ICM2003) [J. Magn. Magn. Mater. **272**, 557 (2004)].

[29] O. K. Andersen, Phys. Rev. B **12**, 3060 (1975).

[30] R. Lizárraga, L. Nordström, L. Bergqvist, A. Bergman, E. Sjöstedt, P. Mohn, and O. Eriksson (unpublished).

[31] R. Lizárraga, Licentiate thesis, Uppsala University 2003 (see www.fysik.uu.se/theomag/).